Supporting information for:

Microporous humins synthesized in concentrated sulfuric acid using 5-hydroxymethyl furfural

Fredrik Björnerbäck[†], Diana Bernin[†,‡], Niklas Hedin[†,*]

[†]Department of Materials and Environmental Chemistry, Arrhenius laboratory, Stockholm University, SE-106 91 Stockholm, Sweden

[‡]present address for Diana Bernin: Department of Chemistry and Chemical Engineering, Chalmers University of Technology, SE-41296 Gothenburg, Sweden

Table of contents

Supplementary figures

Supplementary tables

Supplementary calculations

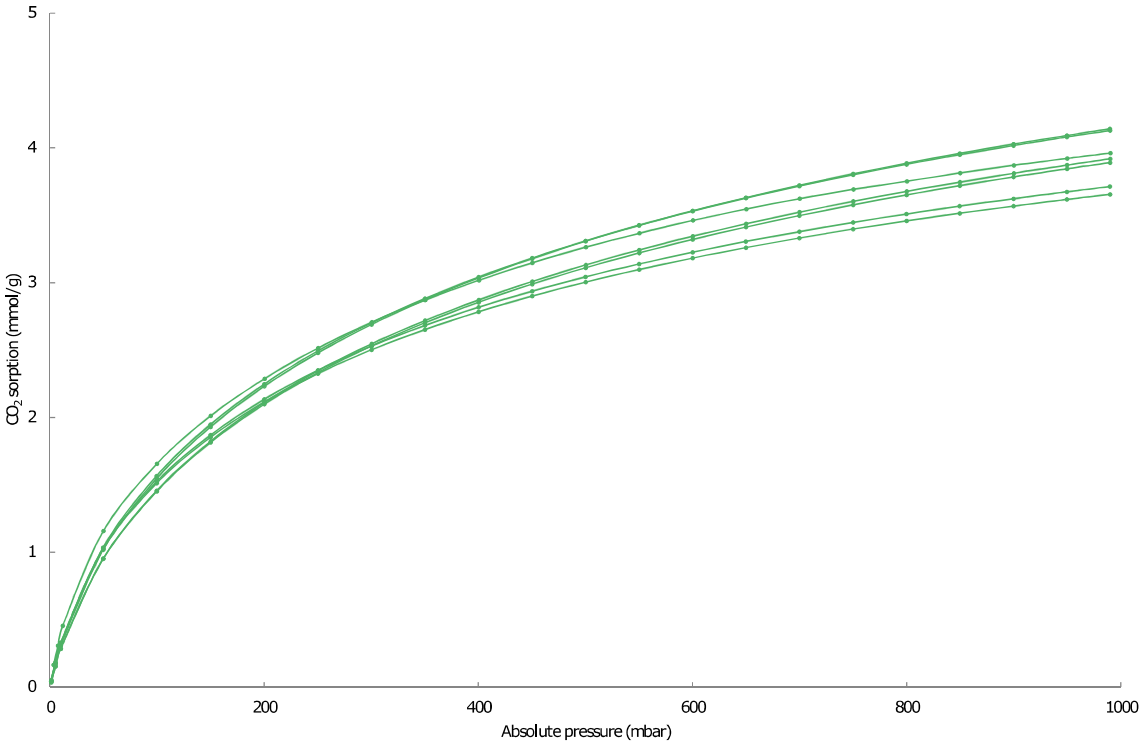

Figure S1. Reproducibility the CO_2 sorption isotherms for seven different MHH-4 samples recorded at 0 °C. Note, the isotherms were recorded on a different device (Micromeritics Gemini VII) than those presented in the main manuscript. The preparation of the samples were performed by degassing in a flow if dry N_2 at a temperature of 400 °C. The data is not directly comparable to the corresponding sorption data presented in the main manuscript; however, it supports the reproducibility of the MHH-4 synthesis.

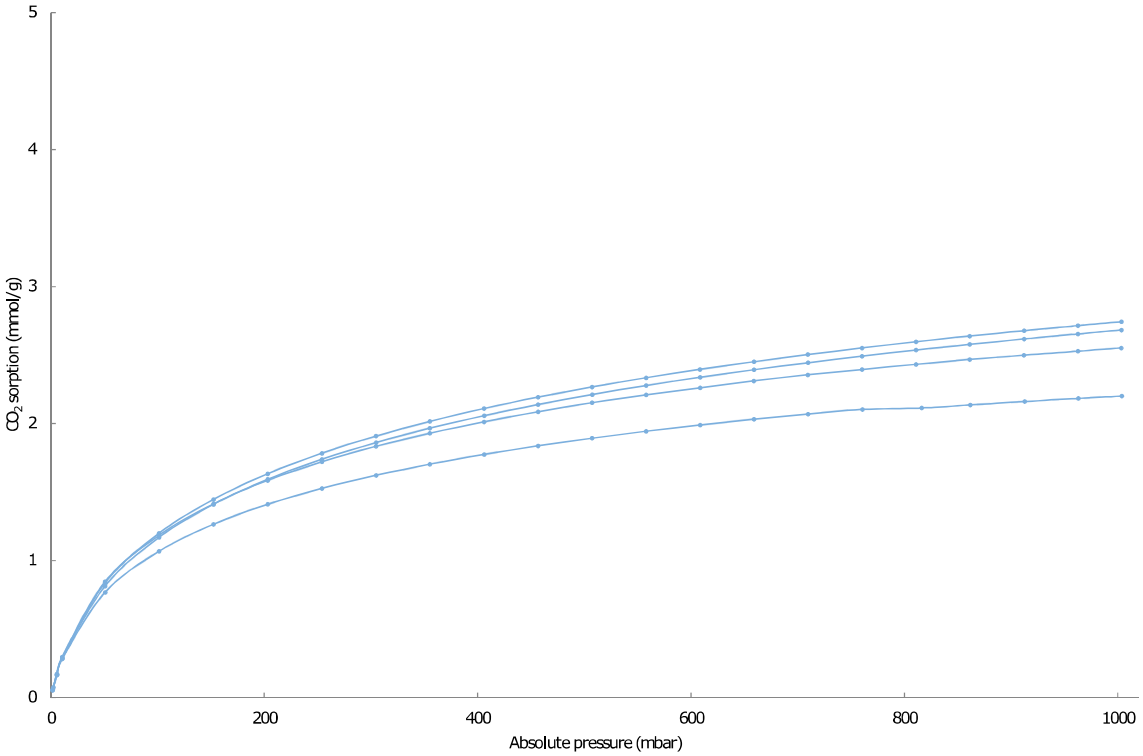

Figure S2. Reproducibility the CO_2 sorption isotherms for four different MHH-2 samples recorded at 0 °C. Note, the isotherms were recorded on a different device (Micromeritics Gemini VII) than those presented in the main manuscript. The preparation of the samples were performed by degassing in a flow if dry N_2 at a temperature of 200 °C. The data is not directly comparable to the corresponding sorption data presented in the main manuscript; however, it supports the reproducibility of the MHH-2 synthesis.

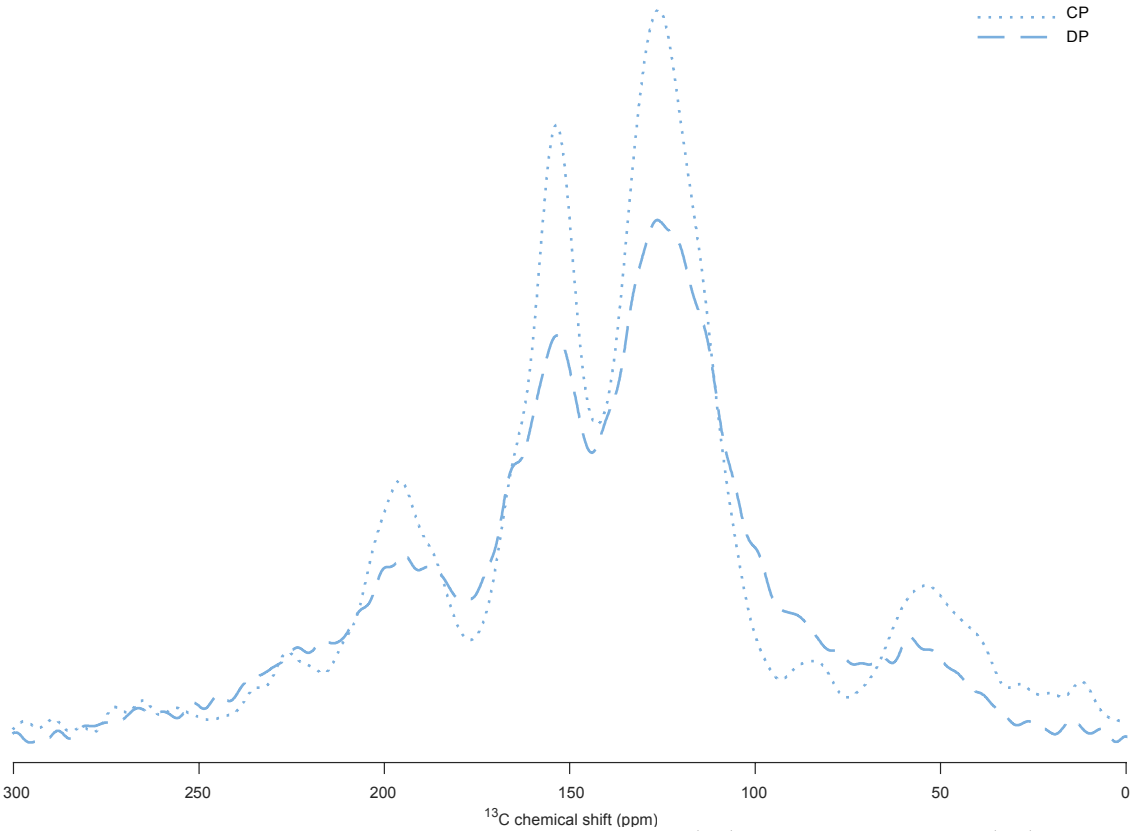

Figure S3. Solid state nuclear magnetic resonance crosspolarization (CP) and direct polarization (DP) spectra for MHH-2.

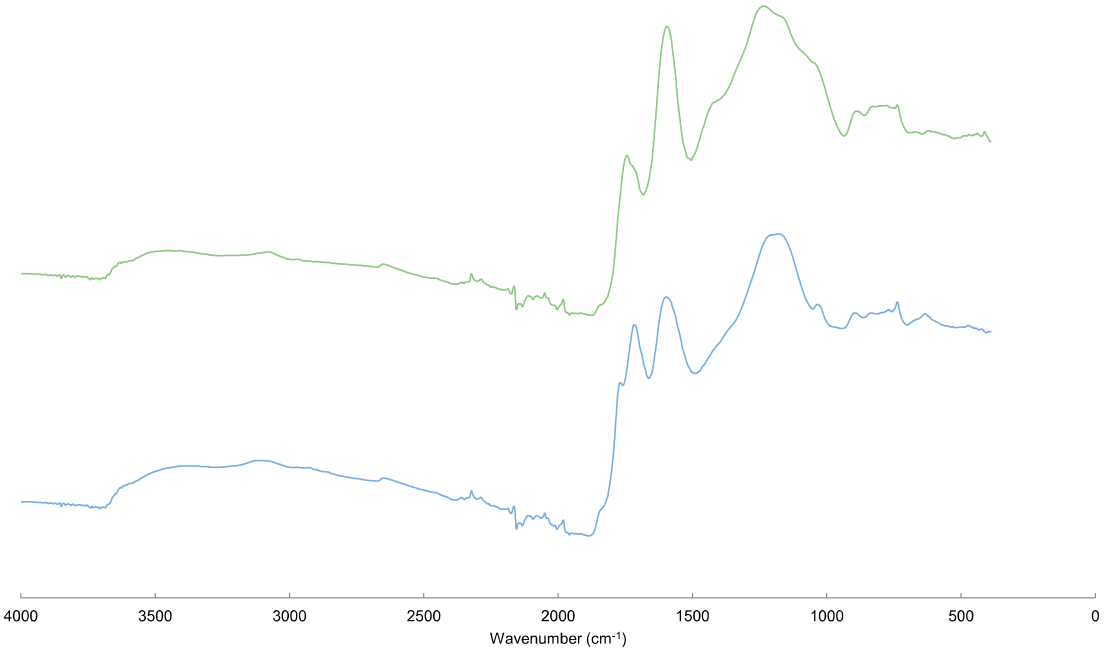

Figure S4. Fourier transform infrared spectra recorded on MHH-2 (blue) and MHH-4 (green) using an attenuated total reflection device and presented in its quasi-absorbance mode.

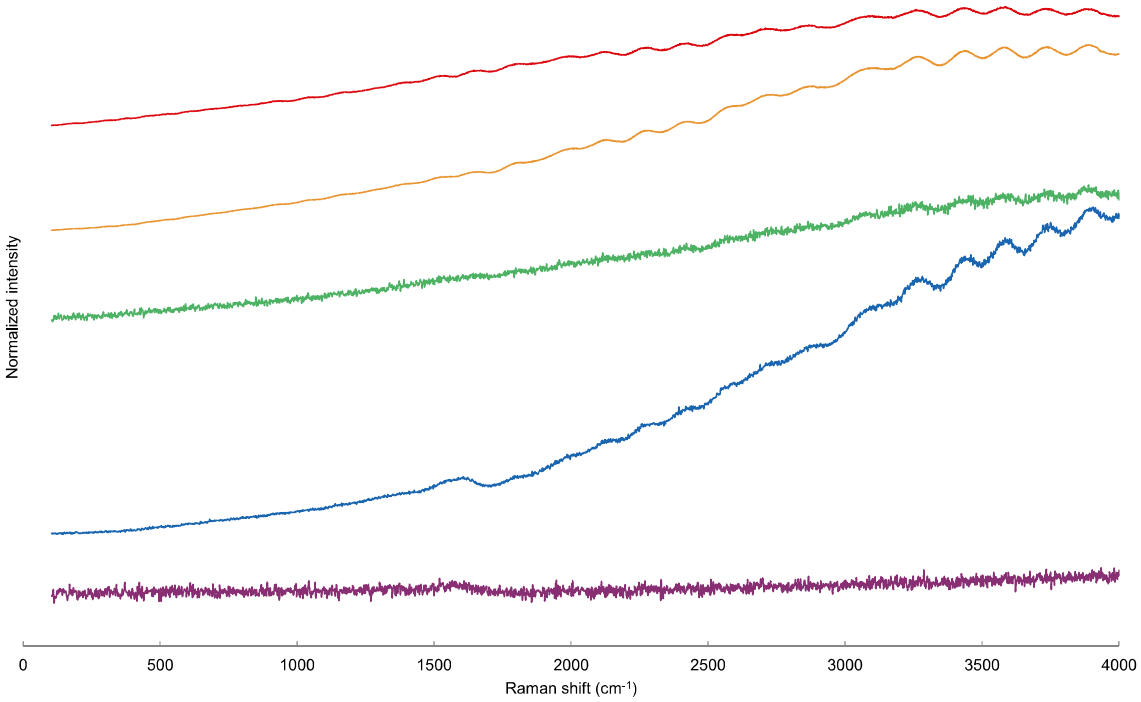

Figure S5. Raman spectra of MHH-2 recorded with an excitation laser wavelength of 532 nm. The analysis was performed sequentially with a focus on the same spot of the sample and with varied laser power. The run order corresponds to the spectra in the figure from the bottom and up with laser powers of 0.005 mW (purple), 0.056 mW (blue), 0.005 mW (green), 0.56 mW (yellow), and 0.056 mW (red).

Figure S6. Raman spectra of MHH-4 recorded with an excitation laser wavelength of 532 nm. The analysis was performed sequentially with a focus on the same spot of the sample and with varied laser power. The run order corresponds to the spectra in the figure from the bottom and up with laser powers of 0.005 mW (purple), 0.056 mW (blue), 0.005 mW (green), 0.56 mW (yellow), and 0.056 mW (red).

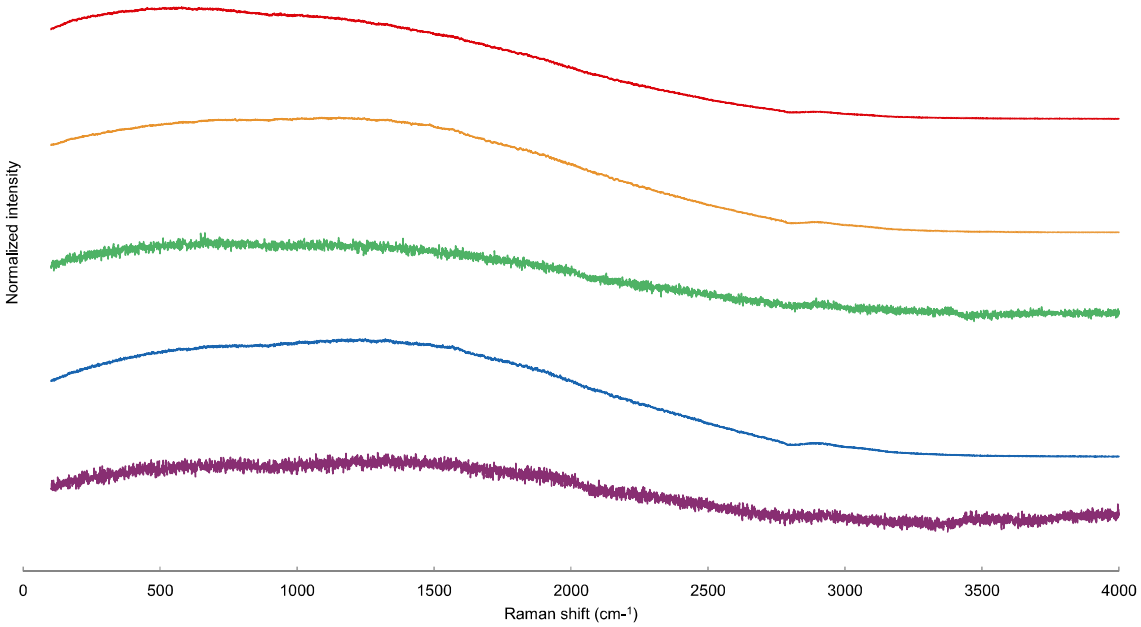

Figure S7. Raman spectra of MHH-2 recorded with an excitation laser wavelength of 785 nm. The analysis was performed sequentially with a focus on the same spot of the sample and with varied laser power. The run order corresponds to the spectra in the figure from the bottom and up with laser powers of 0.0088 mW (purple), 0.088 mW (blue), 0.0088 mW (green), 0.88 mW (yellow), and 0.088 mW (red).

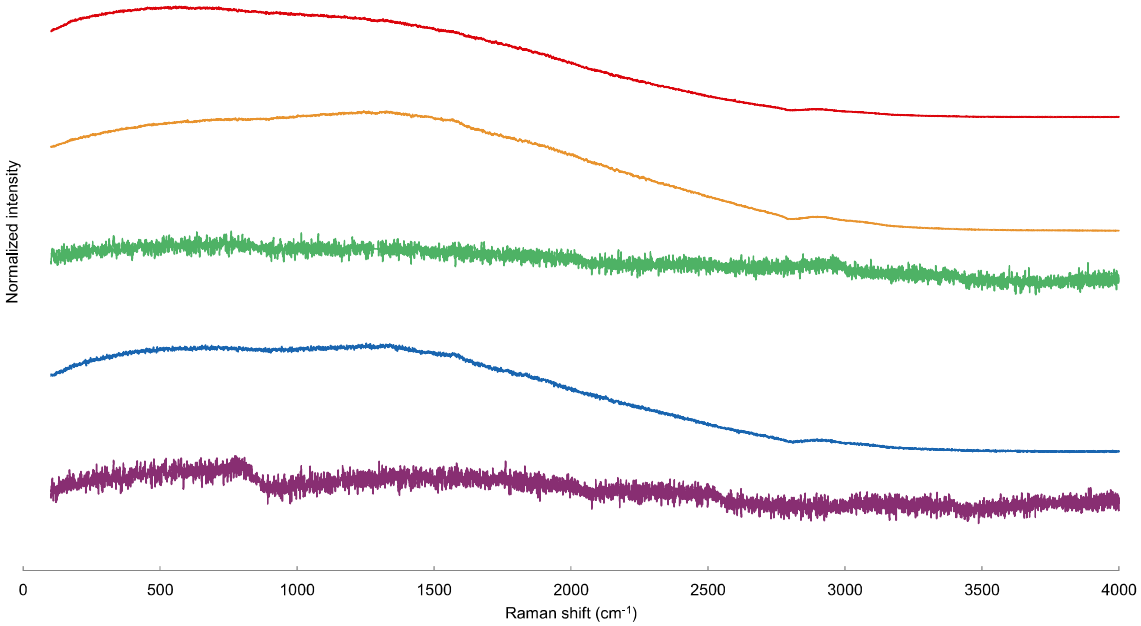

Figure S8. Raman spectra of MHH-4 recorded with an excitation laser wavelength of 785 nm. The analysis was performed sequentially with a focus on the same spot of the sample and with varied laser power. The run order corresponds to the spectra in the figure from the bottom and up with laser powers of 0.0088 mW (purple), 0.088 mW (blue), 0.0088 mW (green), 0.88 mW (yellow), and 0.088 mW (red).

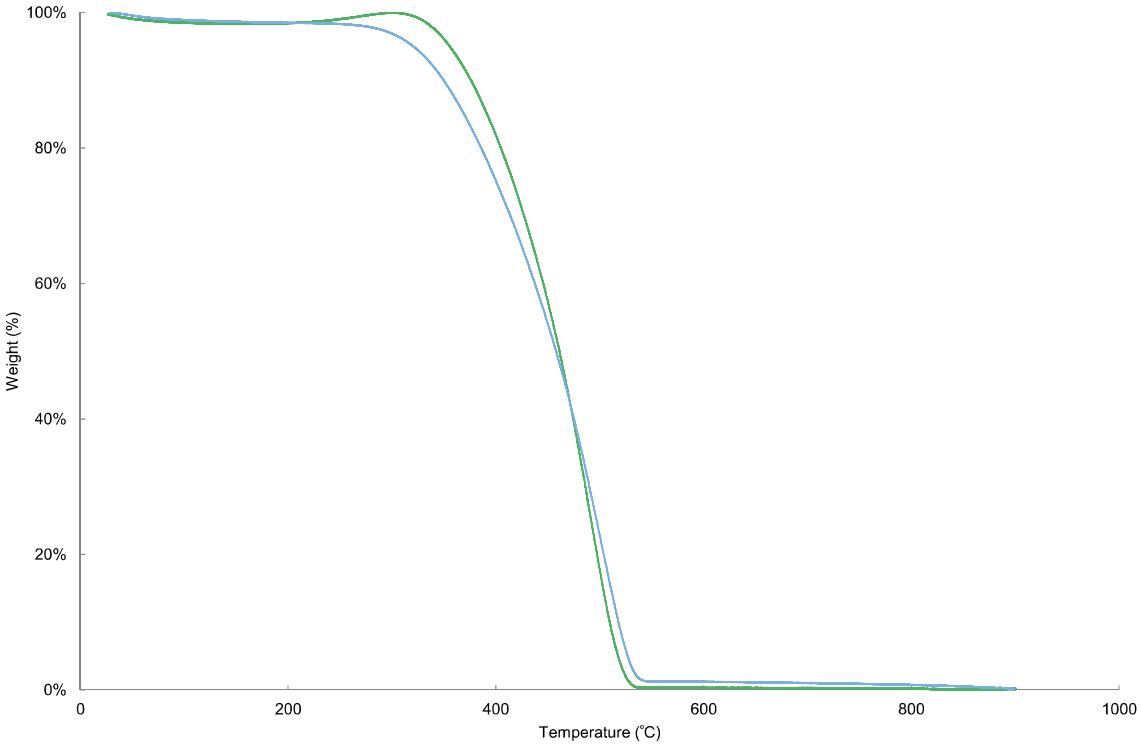

Figure S9. Thermogravimetric analyses of and the MHH-2 (blue) and MHH-4 (green) samples at a heating rate of 1 °C/minute. The experimental data has been normalized.

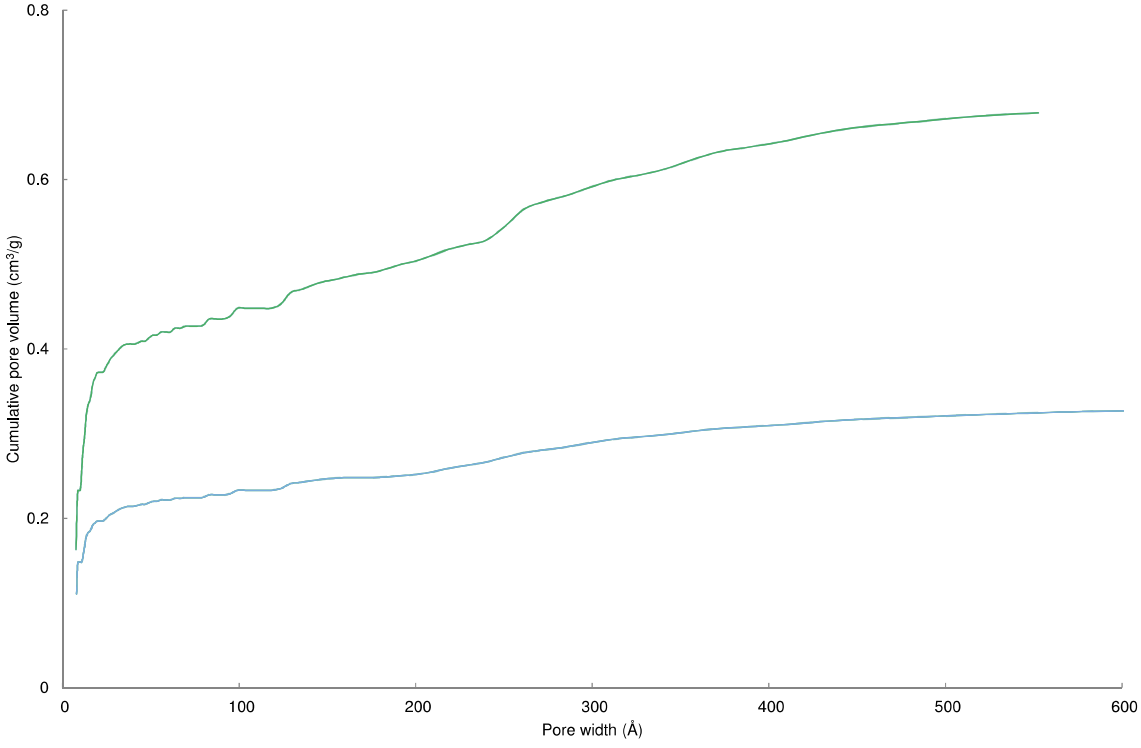

Figure S10. Cumulative pore volume for MHH-2 (blue) and MHH-4 (green) using N_2 adsorption data and a density functional theory through Micromeritics' routines for carbon slit-shaped pores.

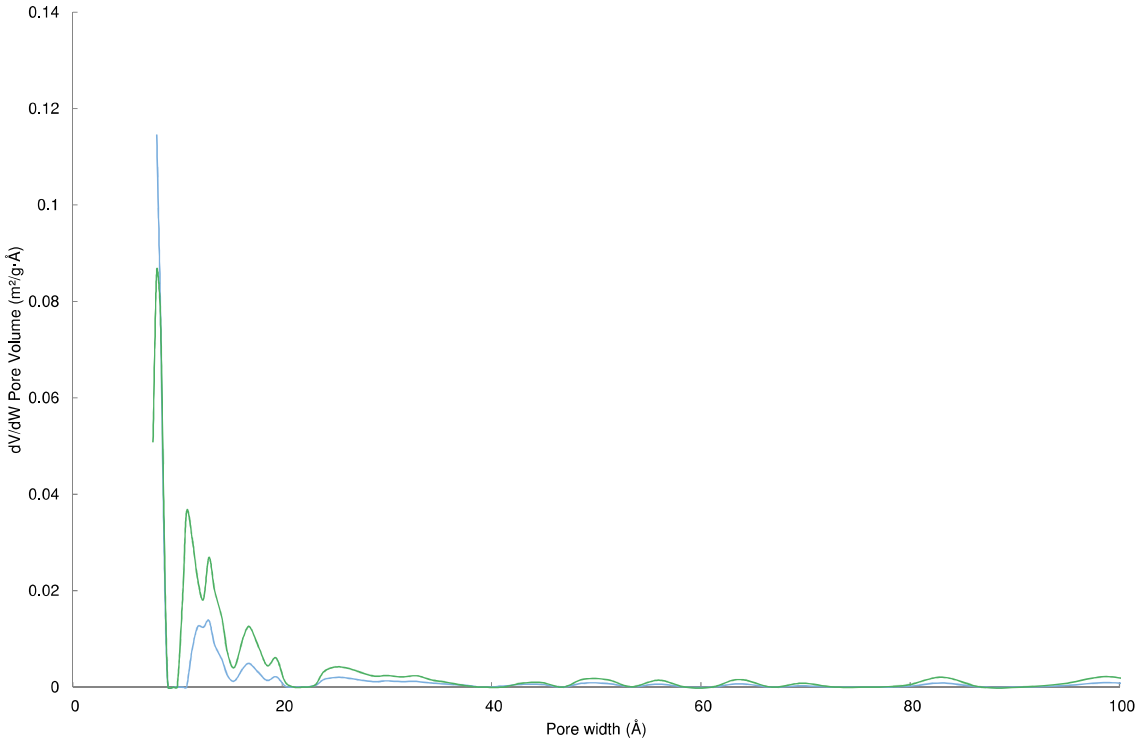

Figure S11. Pore size distributions for MHH-2 (blue) and MHH-4 (green) using N_2 adsorption data and a density functional theory through Micromeritics' routines for carbon slit-shaped pores.

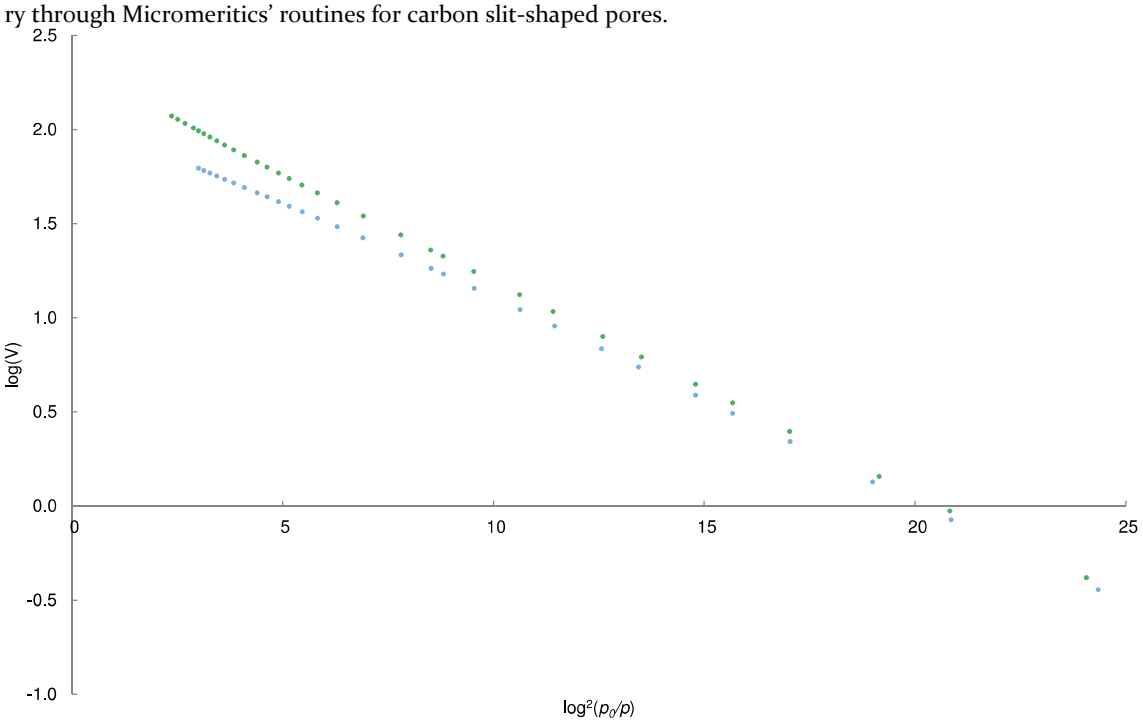

Figure S12. Dubinin-Radushkevich plots using N_2 adsorption data for MHH-2 (blue) and MHH-4 (green) with p/p_o interval $1.24 * 10^{-5}$ - 0.02; corresponding to micropore volumes of 0.25 and 0.39 cm^3/g for MHH-2 and MHH-4, respectively.

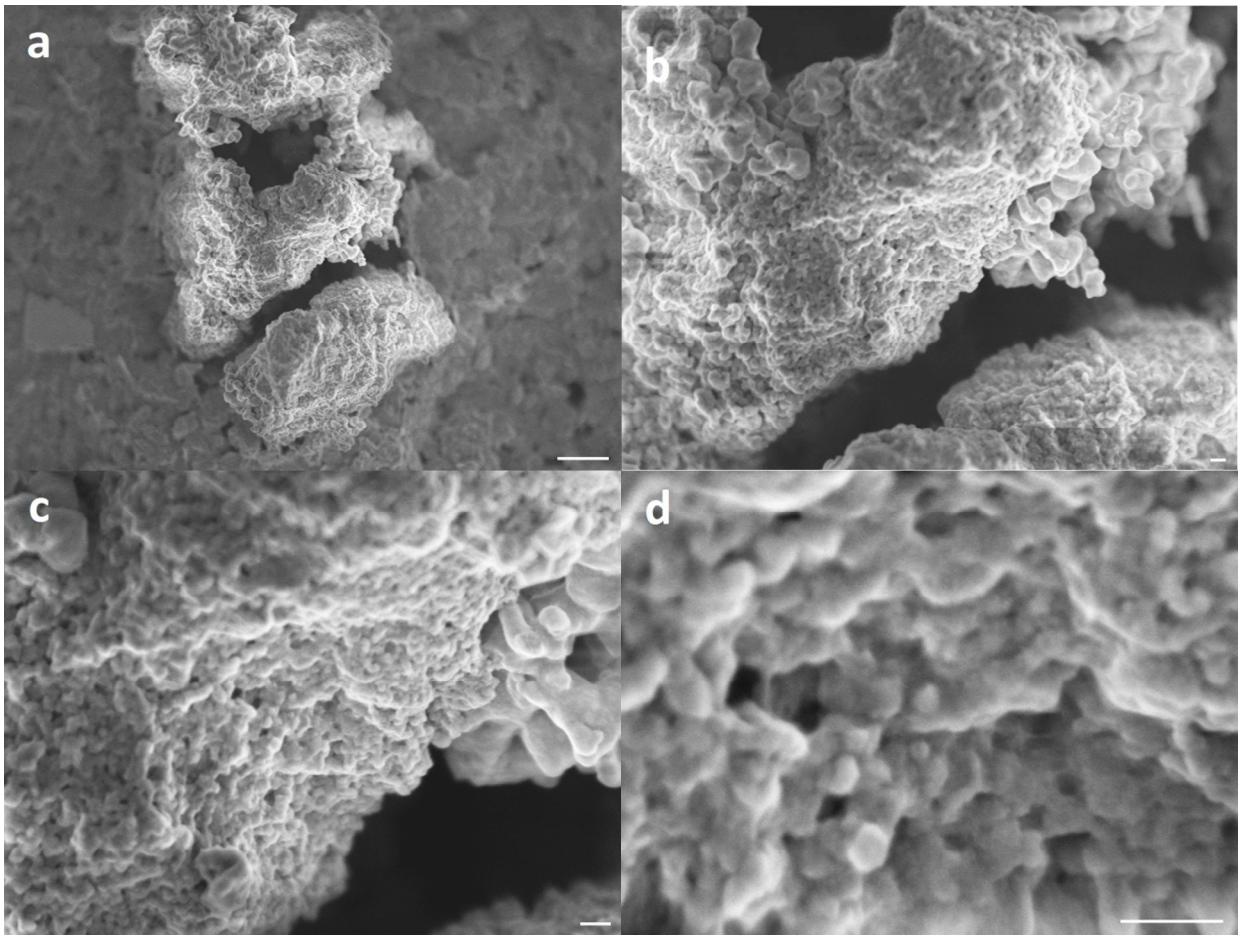

Figure S13. SEM images of one MHH-2 particle. Magnifications of 10,000x with a scale bar of 1 µm (a), 30,000x with a scale bar of 100 nm (b), 60,000x with a scale bar of 100 nm (c) and 200,000x with a scale bar of 100 nm (d).

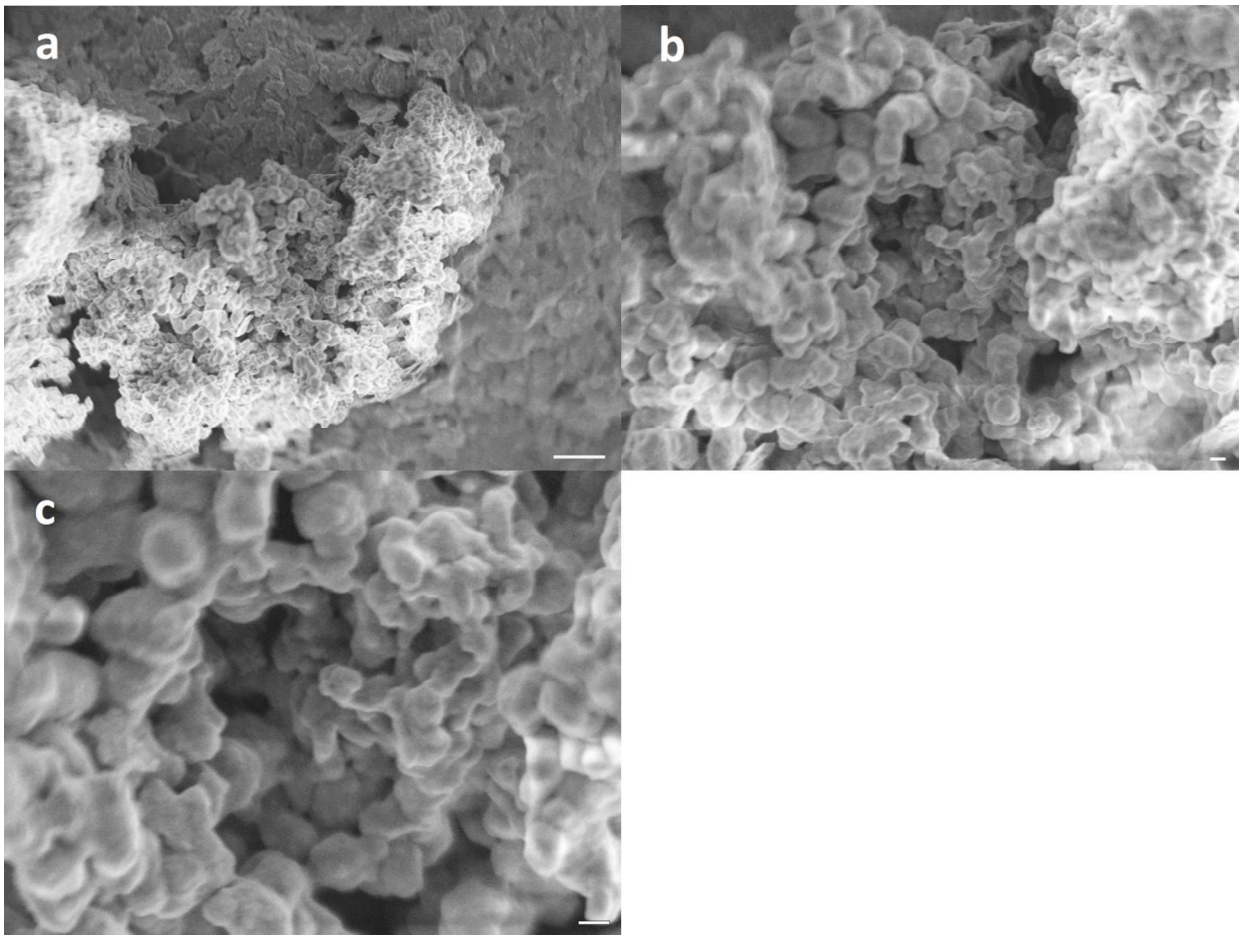

Figure S14. SEM images of a second MHH-2 particle. Magnifications of 10,000x with a scale bar of 1 µm (a), 30,000x with a scale bar of 100 nm (b) and 60,000x with a scale bar of 100 nm (c; same as Figure 5a).

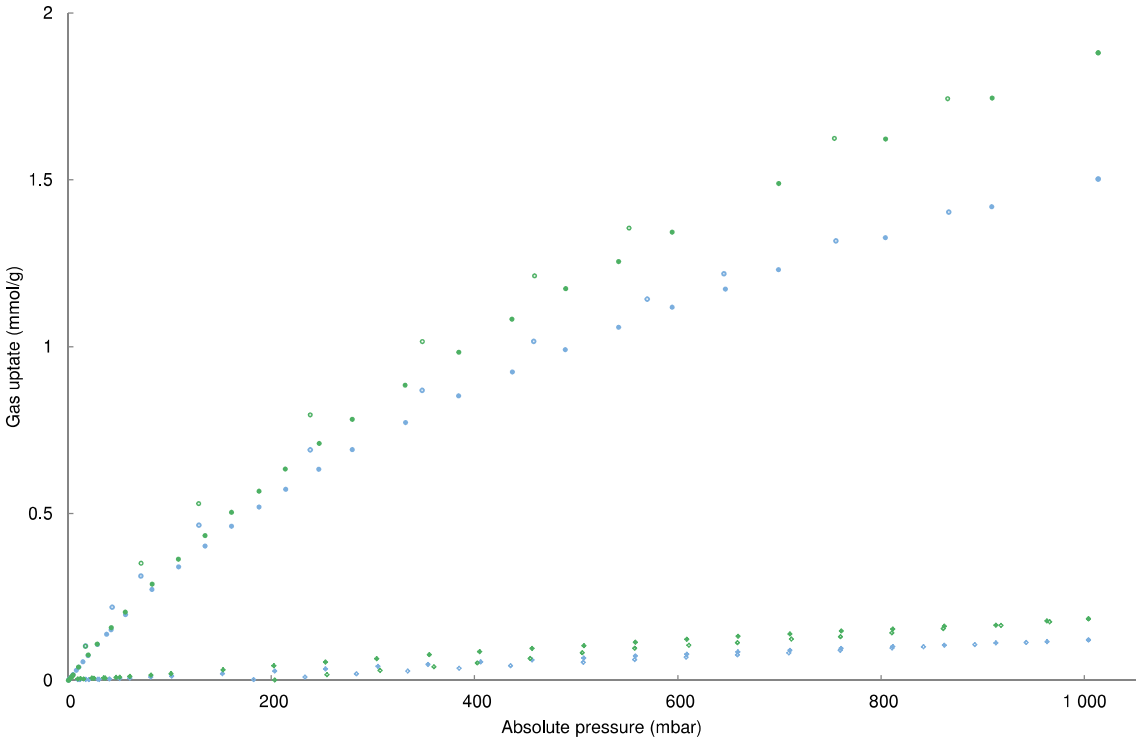

Figure S15. Adsorption and desorption isotherms at 50 °C of N_2 (diamonds) and CO_2 (circles) for MHH-2 (blue) and MHH-4 (green). Filled symbols = adsorption isotherms, empty symbols = desorption isotherms.

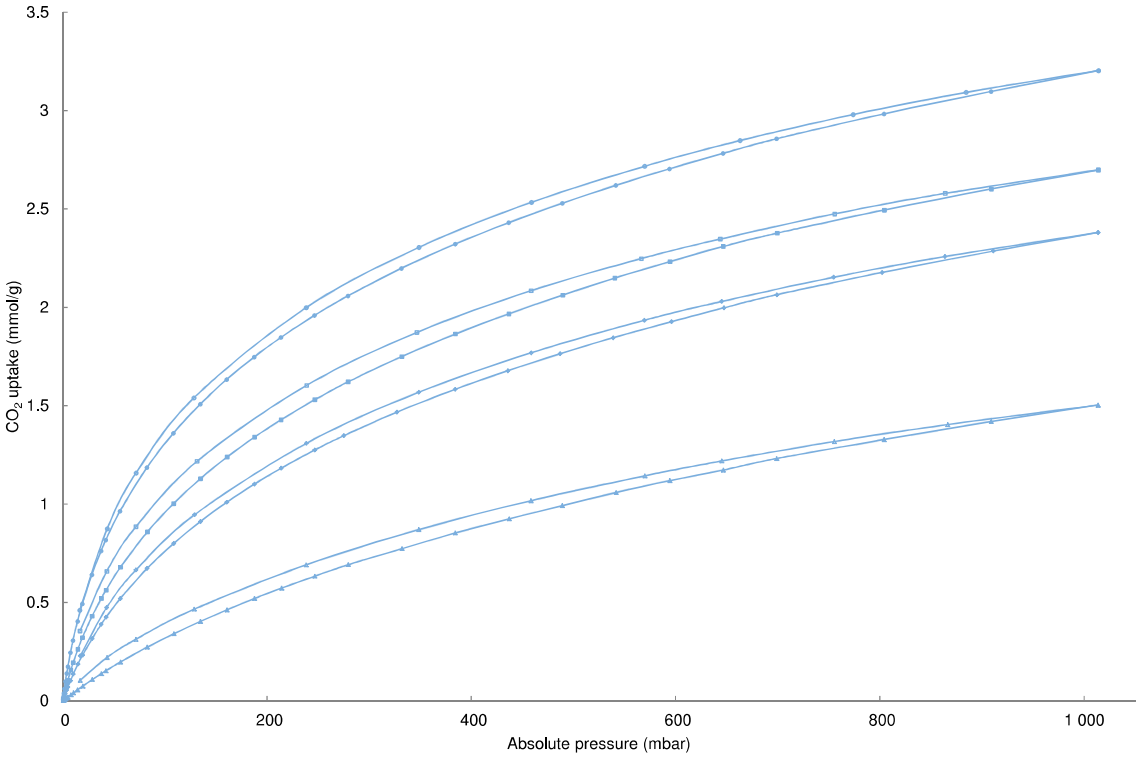

Figure S16. The CO_2 sorption and desorption isotherms recorded at temperatures of 0 (circle), 10 (square), 20 (diamond) and 50 °C (triangle) for MHH-2. Filled symbols = sorption isotherms, empty symbols = desorption isotherms.

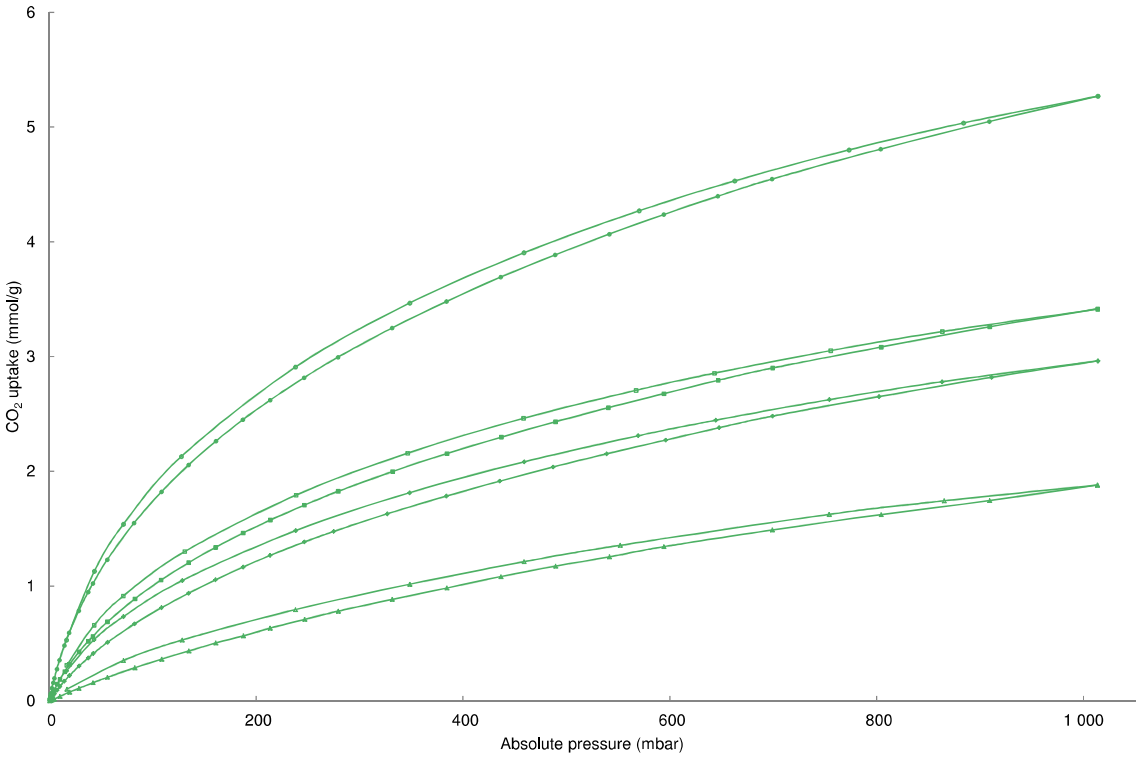

Figure S17. The CO_2 sorption and desorption isotherms recorded at temperatures of 0 (circle), 10 (square), 20 (diamond) and 50 °C (triangle) for MHH-4. Filled symbols = sorption isotherms, empty symbols = desorption isotherms.

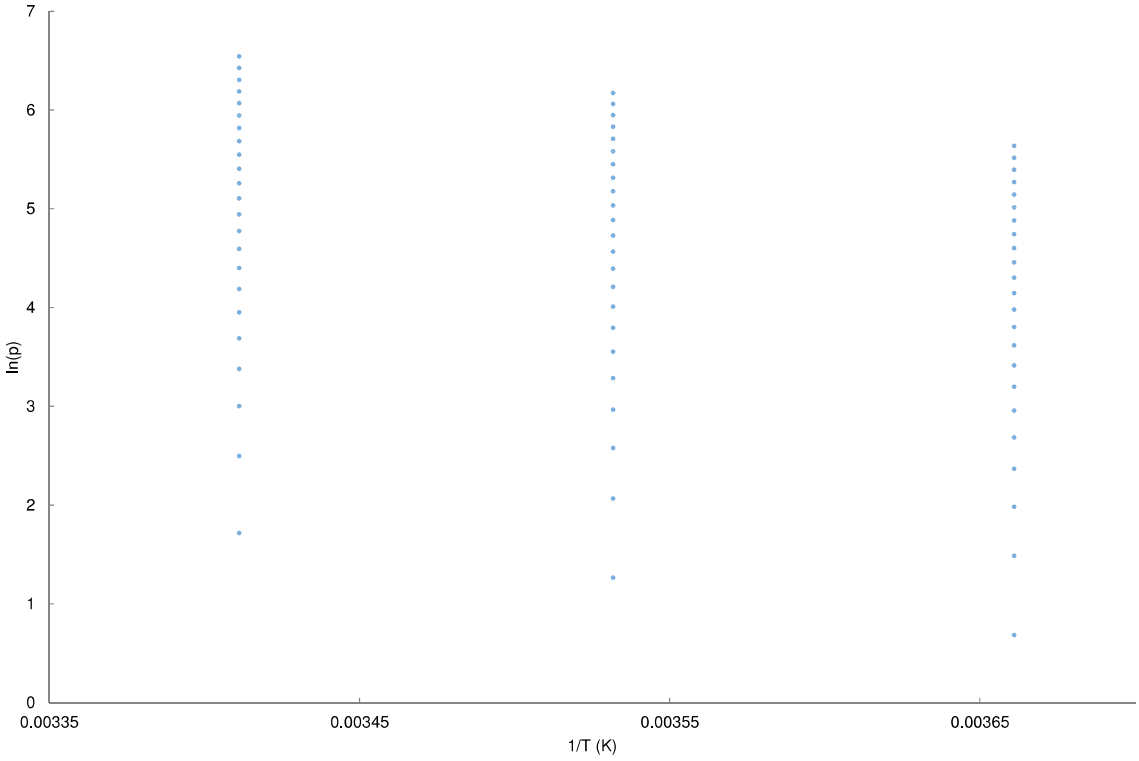

Figure S18. Sorption isosters of CO_2 for MHH-2, calculated from the adsorption isotherm data recorded at temperatures of 0, 10 and 20 °C.

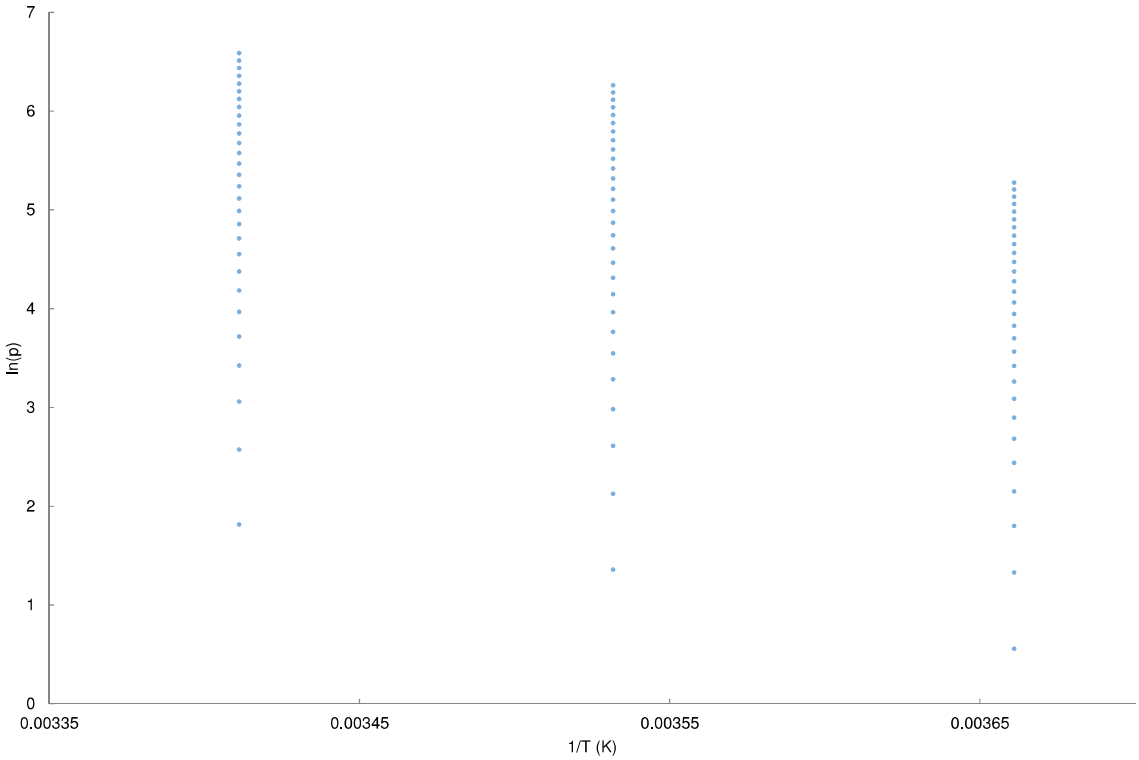

Figure S19. Sorption isosters of CO_2 for MHH-4, calculated from adsorption isotherm data recorded at temperatures of 0, 10 and 20 °C.

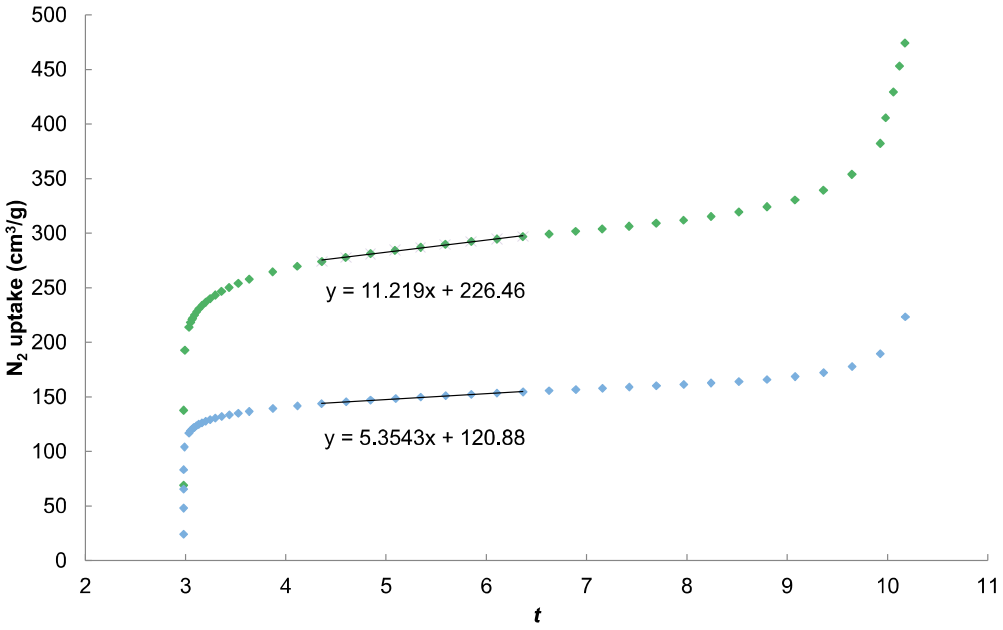

Figure S20. *t*-plot for MHH-2 (blue) and MHH-4 (green) with formulas for linear regressions using selected points.

Table S1. Elemental compositions.

Name, starting material(s), ratio of starting materials, synthesis details etc.	C (wt. %)	H (wt. %)	N (wt. %)	O (wt. %)	S (wt. %)	H/C atomic ratio	O/C atomic ratio	Ref.
MHH-2	60.08	3.05	<0.10	36.18*	0.69	0.60	0.45	This work
MHH-4	73.91	2.81	<0.10	22.86*	0.42	0.45	0.23	This work
Solid acids synthesized with H_2SO_4								
Naphthalene	53.5	1.6	-	24.9	20.0	0.35	0.35	[1]
Lignin	54.3	3.6	2.1	36.2	3.9	0.78	0.50	[2]
HTC of Lapsi seeds	62.1	-	-	-	-	-	-	[3]
HTC of Glucose	79.5	4.3	-	9.8	6.4	0.64	0.09	[4]
Saccharide humins synthesized with H_2SO_4								
HMF	61.2	4.5	-	34.3*	-	0.88	0.42	[5]
Glucose	-	-	-	-	-	0.79	0.36	[6]
Fructose	-	-	-	-	-	0.76	0.36	[6]
Xylose	-	-	-	-	-	0.68	0.33	[6]
Glucose/fructose 1:1	-	-	-	-	-	0.77	0.35	[6]
Glucose/fructose/xylose 1:1:1	-	-	-	-	-	0.74	0.34	[6]
Glucose/HMF 1:0.2	-	-	-	-	-	0.76	0.34	[6]
Glucose/1,2,4-trihydroxybenzene 1:0.2	-	-	-	-	-	0.70	0.39	[6]
Glucose/1,2,4-trihydroxybenzene 1:0.01	-	-	-	-	-	0.78	0.39	[6]
Glucose	66.4	4.7	-	28.9	-	0.84	0.33	[7]
Mannose	65.7	4.7	-	29.6	-	0.85	0.34	[7]
Galactose	66.1	4.7	-	29.2	-	0.85	0.33	[7]
Arabinose	68.3	4.9	-	26.8	-	0.85	0.29	[7]
Cellobiose	65.1	5.1	-	29.8	-	0.93	0.34	[7]
Methyl-α-glucose	66.1	4.9	-	28.9	-	0.88	0.33	[7]
Glucose, 180 °C, 0.01M H_2SO_4, Helium, various heat treatments. Data adapted from figure in ref. [8]								
Glucose, 180 °C, 0.01M H_2SO_4, Helium	66.3	4.4	-	29.3	-	0.79	0.33	[8]
110 °C	-	-	-	-	-	0.8	0.34	[8]
400 °C	-	-	-	-	-	0.6	0.21	[8]
500 °C	-	-	-	-	-	0.5	0.16	[8]
600 °C	-	-	-	-	-	0.38	0.07	[8]
700 °C	-	-	-	-	-	0.28	0.05	[8]
Saccharide humins								
HMF, 27.5 MPa, 290-400 °C.	57.1	4.8	-	38.1	-	1.00	0.50	[9]
HMF, 190 °C, pH 2.5	58	3.0	-	39*	-	0.62	0.50	[10]
Glucose, 190 °C, pH 2	62	-	-	-	-	-	-	[10]
Glucose, 190 °C, pH 4	58	-	-	-	-	-	-	[10]
Humins, based on 26 samples from soil. Details and Van Krevelen diagram in ref. [11]								
Soil humins (range)	48-62	4.2-7.3	0.9-6.0	28-45	0.1-0.9	0.82-1.72	0.37-0.61	[11]
Activated carbons, pyrolysis or physical activation								
Rice husk, 350 °C, Ar	44.2	2.5	0.65	17.0*	-	0.67	0.29	[12]
Rice husk, 450 °C, Ar	45.5	1.9	0.65	11.6*	-	0.50	0.19	[12]
Rice husk, 550 °C, Ar	47.0	2.0	0.68	8.1*	-	0.51	0.13	[12]
Palm shell, 700 °C, N_2	83.6	0.8	0.6	15.0*	-	0.11	0.13	[13]
Palm shell, 700 °C, N_2, 800 °C, CO_2	87.1	1.0	1.1	10.8*	-	0.14	0.09	[13]
Activated carbons, chemical activation								
Rice husk, 350 °C, Ar, KOH, 750 °C	67.1	2.3	0.39	18.9*	-	0.41	0.21	[12]
Rice husk, 450 °C, Ar, KOH, 750 °C	80.7	0.6	0.27	9.0*	-	0.09	0.08	[12]
Rice husk, 550 °C, Ar, KOH, 750 °C	77.3	1.0	0.44	7.7*	-	0.15	0.07	[12]
Tea waste, H_3PO_4, micro-	66.2	3.8	1.63	28.4	-	0.68	0.32	[14]

wave, 300 °C, N_2								
Tea waste, H_3PO_4, micro-wave, 350 °C, N_2	76.3	3.2	1.44	19.0	-	0.50	0.19	[14]
Tea waste, H_3PO_4, micro-wave, 550 °C, N_2	79.3	2.5	1.43	16.8	-	0.38	0.16	[14]
Tea waste, H_3PO_4, micro-wave, 700 °C, N_2	70.0	1.8	2.10	26.1	-	0.31	0.28	[14]
Palm shell, H_2SO_4, 700 °C, N_2	83.3	0.4	0.2	16.1*	-	0.06	0.15	[13]
Almond shell, $ZnCl_2$, 750 °C, N_2	79.2	0.64	-	28.1*	-	0.10	0.27	[15]
Apricot stones, $ZnCl_2$, 800 °C, N_2	76.0	0.49	-	23.5*	-	0.08	0.23	[15]
Hazelnut shell, $ZnCl_2$, 750 °C, N_2	72.0	1.8	-	26.2*	-	0.30	0.27	[15]
Walnut shell, $ZnCl_2$, 750 °C, N_2	75.3	0.71	-	24.0*	-	0.11	0.24	[15]

**Oxygen content for samples MHH-2 and MHH-4 and other samples was calculated as the remainder.*

Table S2. CO_2 and CH_4 uptake (mmol/g), and apparent selectivities. Apparent selectivities are defined as $(n_{CO_2}/n_x)/(P_{CO_2}/P_x)$, where x = N_2 or CH_4, or $(n_{CH_4}/n_{N_2})/(P_{CH_4}/P_{N_2})$.

Name	MHH-2	MHH-4
CO_2 uptake, 1 bar, 0 °C	3.20	5.27
CO_2 uptake, 0.15 bar, 0 °C	1.58	2.18
CO_2 uptake, 1 bar, 50 °C	1.50	1.88
CO_2 uptake, 0.15 bar, 50 °C	0.44	0.59
CH_4 uptake, 1 bar, 0 °C	1.06	2.09
CH_4 uptake, 0.5 bar, 0 °C	0.70	1.32
CO_2/N_2 Selectivity, 0 °C, P_{CO_2}=0.15, P_{N_2}=0.85	29.8	18.2
CO_2/N_2 Selectivity, 50 °C, P_{CO_2}=0.15, P_{N_2}=0.85	23.8	20.7
CO_2/CH_4 Selectivity, 0 °C, $P_{CH_4}=P_{CO_2}$=0.5	3.6	3.0
CH_4/N_2 Selectivity, 0 °C, $P_{CH_4}=P_{N_2}$=0.5	3.6	3.0

Table S3. CO_2 uptake, selectivity and heat of adsorption comparison to other organic porous sorbents. Data were compiled from reviews and research papers.[16–26] (Note: typically higher adsorption is observed at lower temperature).

Name	CO_2 uptake, 1 bar, 0 °C	CO_2 uptake, 0.15 bar, 0 °C	Q_{st} (kJ/mol)	CO_2-over-N_2 selectivity	Selectivity type
MHH-2	3.2	1.58	32	23	0 °C, 1 bar, IAST
MHH-4	5.27	2.18	43	65	0 °C, 1 bar, IAST
Porous polymers					
HAT-CTF-450/600	6.3		27		
PPF-1	6.07	1.8			
P-PCz	5.57		30.9		
ALP-1	5.36		29.2	40	0 °C, 1 bar, IAST
BILP-4	5.34	1.99			
TBILP-2	5.18		29		
BILP-3	5.11		28.6		
CPOP-1	4.82	0.97	27	25	0 °C, 1 bar, not specified
PCTF-4	4.66		30		
APOP-3	4.54		27.5		
TNP4	4.45		36.5		
SNU-C1-sca	4.38		31.2		
Fe-POP-1	4.3	1.48			
PINK	4.3		28.9		
fl-CTF350	4.28		32.7		
NOP-50A	4.27		46.7		
mPMF-5	4.25	1.93			
POF-1B	4.19	1.51			
C1M3-Al	4.11		20.9		
TSP-2	4.1		30.2		
Network4	3.96		30		
MOP-C	3.86	1.08			
CPOP-13	3.82		34.2		
HPF-1	3.8		26	120	30 °C, 1 bar, IAST
Azo-CMP1	3.72		30		
TCP-B	3.66		24		
TAPOP-1	3.5		27.8		
PECONF-3	3.49	1.3	26	77	0 °C, Ratio of Henry's law constants
PAN-T	3.36		36.3		
POM2-IM	3.3		31.1		
PAF-18-OLi	3.27		29.5	129	0 °C, 1 bar, IAST
NAB-2	3.19		23		
Azo-MOP-2	3.06				
Tet-4	3.03				
NPOF-4-NH_2	2.9		30.1		
Azo-COP-2	2.55		24.8		
PON-1	2.48				
DA-CMP1	2.28		30		
SNW-1	2.2		35		
PPN-6-CH_2-DETA			55		
PPN-6-SO_3NH_4			40	796	40 °C, 1 bar, IAST

Activated carbons (ACs)						
Name	CO_2 uptake, 1 bar (mmol/g)	Temperature (°C)	CO_2 uptake, 0.15 bar (temperature, °C) (mmol/g)	Q_{st} (kJ/mol)	CO_2-over-N_2 selectivity	Selectivity type
AC petroleum pitch VR-5-M	8.6	0			2.8	
AC pine-nut shell	7.7	0	3.3 (0)	23-42		

AC starch and gelatin	7.5	0		28-63	98	Initial slopes
AC HTC algae	7.4	0		25	10	
TiC-CDC	7.1	0				
AC bamboo	7.0	0	2.5 (0)			
AC template CEM-750	6.9	0				
AC HTC sawdust	6.6-6.1	0	2.0 (0)		5.4	
AC petroleum pitch DO-88-M	6.5					
AC palm shell	6.3	0	2.6 (0)			
MAC-E-7	6	0	1.8 (0)	30	3.8	IAST
AC coconut shell	5.6	0	2.0 (0)			
AC fungi	5.5	0	1.5 (0)			
AC chitosan	5.0	0	2.2 (0)			
AC from HTC	4.82	25				
AC yeast	4.8	25	1.3 (25)			
AC olive stone	4.8	0				
IBN9-NC1-A	4.5					
AC PAN fiber	4.4	25				
Celtuce leaf	4.36					
AC evaporation	4.3	25			30	
AC bean dreg	4.2	25	1.4 (25)			
KNC-A-K	4.05	25			48	IAST
AC from polypyrole	4.02	25				
AC-2-635	3.86					
AC from CER	3.73	25				
AC phenolic resin	3.59	25				
AC-1-600	3.57					
AC from PVF	3.52	25				
3C-1000N	3.25					
AC	3.23	25				
N-rich AC	3.2					
AC silica template	3.2	25			6.5	
AC soft templating	3	5			12.8	
AC olive stone	3	25				
AC-F30/470	2.86	15				
AC almond shell	2.7	25				
AC	2.61	25				
AC amidoxime	2.48	25			22.4	
AC Norit RB1	2.46	21				
AC	2.45	15				
AC macroalgae	2.4	0				
AC	2.25	25				
AC melamine-formaldhyde	2.25	25				
NiO-AC	2.24	25				
AC almond shell	2.11					
AC from Alfa aesar	2.1					
AC	2.07	25				
AC-A35/4	2	20				
AC from ILP	1.95	25				
H-600	1.73					
AC	1.53	25				
Anthracite AC	1.38	30				
AC-RB	1.22	30				

Table S4. Regression analyses of adsorption data and associated parameters for the parametrization of the adsorption data used in the IAST calculations. The coefficients a, b, c, and d relate to single and double component Langmuirians.

Name	Temp (K)	Gas	R-square	a	Conf. 95%	b	Conf. 95%	c	Conf. 95%	d	Conf. 95%
MHH-2	273	CO_2	0.9999	3.353	±0.062	0.001439	±0.000158	1.246	±0.092	0.0249	±0.00232
MHH-2	283	CO_2	1.0000	3.242	±0.039	0.001285	±0.000096	0.9047	±0.0623	0.01883	±0.00147
MHH-2	293	CO_2	1.0000	3.139	±0.039	0.001005	±0.000072	0.8544	±0.0551	0.01264	±0.00081
MHH-2	323	CO_2	1.0000	3.077	±0.101	0.0005182	±0.000077	0.5421	±0.1092	0.004449	±0.000581
MHH-4	273	CO_2	1.0000	7.335	±0.148	0.001028	±0.000083	1.585	±0.110	0.02035	±0.00178
MHH-4	283	CO_2	1.0000	5.454	±0.112	0.0008323	±0.000059	0.9732	±0.0646	0.01537	±0.00118
MHH-4	293	CO_2	1.0000	5.326	±0.120	0.0007195	±0.000054	0.7782	±0.0666	0.01143	±0.00102
MHH-4	323	CO_2	1.0000	4.795	±0.478	0.0004501	±0.000171	0.4636	±0.3688	0.003968	±0.00212
MHH-2	273	CH_4	0.9997	2.068	±0.068	0.001014	±0.000054				
MHH-4	273	CH_4	0.9999	4.798	±0.105	0.0007591	±0.0000249				
MHH-2	273	N_2	0.9999	3.278	±0.129	0.0003031	±0.0000146				
MHH-2	323	N_2	0.9978	3.278	FIXED	3.943E-5	±0.049E-5				
MHH-4	273	N_2	0.9999	3.285	±0.116	0.0003022	±0.0000130				
MHH-4	323	N_2	0.9962	3.285	FIXED	6.145E-5	±0.1E-5				

Table S5. Heat of sorption determined from parameterized isosters (y=lnp, x=1/T) of MHH-2. ($y = ax^2 + bx + c$)

Quantity Adsorbed (mmol/g)	a	b	c	Heat of sorption (kJ/mol)
0.1	-3032744	17320	-22.073	34.2
0.2	-3597326	21398	-28.634	33.5
0.3	-4368249	26814	-37.633	33.7
0.4	-4786918	29807	-42.597	33.4
0.5	-5196255	32736	-47.514	33.2
0.6	-5270195	33286	-48.268	32.9
0.7	-5395659	34201	-49.693	32.7
0.8	-5473799	34771	-50.516	32.5
0.9	-5562748	35430	-51.533	32.3
1	-5588124	35636	-51.760	32.1
1.1	-5636748	36001	-52.271	31.9
1.2	-5595843	35736	-51.682	31.7
1.3	-5675251	36315	-52.581	31.5
1.4	-5581080	35672	-51.336	31.3
1.5	-5533120	35348	-50.645	31.2
1.6	-5376706	34255	-48.601	31.1
1.7	-5384882	34334	-48.640	30.9
1.8	-5496852	35151	-49.999	30.7
1.9	-5513932	35293	-50.159	30.6
2	-5531736	35451	-50.373	30.3
2.1	-5293292	33797	-47.389	30.0
2.2	-4795446	30275	-41.046	30.1
2.3	-4307403	26837	-34.879	30.0

The coefficients a, b, and c are presented with more numbers than are significant. Our estimation is that we can express the heat of sorption with three significant numbers.

Table S6. Heat of sorption determined from parameterized isosters (y=lnp, x=1/T) of MHH-4.

Quantity Adsorbed (mmol/g)	a	b	c	Heat of sorption (kJ/mol)
0.1	-9691340	63506	-102.04	41.4
0.2	-9803781	64351	-102.86	41.0
0.3	-10240328	67382	-107.63	41.5
0.4	-11184468	73997	-118.85	41.9
0.5	-11863976	78788	-126.99	42.0
0.6	-12766670	85152	-137.95	42.2
0.7	-13007702	86846	-140.70	42.2
0.8	-13401856	89623	-145.40	42.3
0.9	-13944835	93449	-151.95	42.4
1	-14344100	96272	-156.78	42.4
1.1	-14922461	100369	-163.88	42.3
1.2	-15517535	104580	-171.19	42.3
1.3	-15962006	107723	-176.61	42.3
1.4	-16296049	110077	-180.63	42.3
1.5	-16525711	111696	-183.36	42.4
1.6	-16723248	113086	-185.69	42.4
1.7	-17002769	115049	-189.03	42.5
1.8	-17174147	116251	-191.04	42.6
1.9	-17498850	118546	-194.99	42.6
2	-17967011	121854	-200.73	42.6
2.1	-18312143	124300	-204.97	42.5
2.2	-18635275	126581	-208.90	42.5
2.3	-19025875	129350	-213.72	42.5
2.4	-19485564	132620	-219.45	42.3
2.5	-19713032	134234	-222.24	42.2
2.6	-19762327	134565	-222.71	42.4
2.7	-19741052	134401	-222.32	42.5
2.8	-19639635	133674	-220.94	42.6
2.9	-19614918	133474	-220.47	42.8

The coefficients a, b, and c are presented with more numbers than are significant. Our estimation is that we can express the heat of sorption with three significant numbers.

IAST calculations

Adsorption data was analyzed with Matlab's curve "fitting" routines using "custom equations" and the "Levenberg-Marquart" algorithm where the summed square deviations inbetween predicted adsorption and experimentally determined were minimized. For the CO_2 adsorption isotherms a two-component Langmuirian model was used, and for the N_2 and CH_4 adsorption a regular single-component Langmuir model was used.

Langmuir equation: y=abx/(1+bx); y is the adsorptive uptake, x is the pressure, and a and b are parameters.

Langmuir two-component: y= abx/(1+bx)+ cdx/(1+dx), y is the adsorptive uptake, x is the pressure, and a and b are parameters.

The regression analyses were used as parameterization of the adsorptive uptake as expressed with the single- and two-component Langmuir equations. The values of the parameters are shown in Table S3 and used to parametrize the adsorption in the subsequent IAST modelling. The regression analyses of the adsorption data led to very high R-values as expected, but also the relatively wide 95%-confidential intervals of the involved parameters highlighted the importance of high quality adsorption data for IAST modelling. The error estimation was preformed from the variations in-between data and the model using Matlab's routines.

It was not possible to lock the amounts for the both components in the two-component Langmuir model for the CO_2 adsorption, which indicates that this model is not fully accurate. For the N_2 uptake, the max amount was locked to the value as determined at a temperature of 273K also for the temperature of 323K. The Toth-Langmuir combination was tested but did not produce robust results. The parameters from the associated regression analyses are presented in Table S3.

The IAST modelling was performed by using an in-house written code in Matlab. Shortly describe, in this code the Matlab's fsolve function was used to numerically solve the underlying equation in the IAST model by equating the corresponding pressure- and uptake-dependent integrals for the involved gas molecules. These codes can be supplied from the authors upon request.

For the CO_2/N_2 gas pair the adsorptive selectivities were estimated with IAST using single component data recorded at 273 K and 323 K. The IAST calculations were performed with parametrized data. The estimated binary uptake (CO_2 over N_2) is not reported but the binary selectivity is presented in the main manuscript as a function of the partial pressure of CO_2 in the gas phase (y_{CO_2}). For the CO_2/CH_4 gas pair, IAST calculations were performed with parametrized adsorption data recorded at 273 K. The binary selectivity is presented in the main manuscript as a function of y_{CO_2}. In a similar IAST calculations for the CH4-over-N selectivity was performed with parametrized adsorption data recorded at 273 K.

Binary uptake: $S_1 = n(_{CO_2,\ IAST})/n(_{N_2,\ IAST})$; n_x = amount (mol) of gas adsorbed on the solid from a binary gas mixture.

Binary selectivity: $S_{12} = n(_{CO_2,\ IAST})/n(_{N_2,\ IAST}) * (p_{N_2}/p_{CO_2})$; p_x = the partial pressure of x in the gas mixture.

The S_{12} are presented as a function of the fraction of CO_2 in the gas phase (y_{CO_2}) and calculated with the IAST. Apparent selectivities are presented in the Table S2 to allow for comparison with literature data.

Heat of sorption calculations

The CO_2 adsorption isotherm data recorded at temperatures of 0, 10 and 20 °C were replotted as isosteres; In that representation, the values of ln(p) were plotted as a function of 1/T at defined adsorbed quantities (c.f. Figure S17 and S18). The heat of adsorption is proportional to the derivative of ln(p) with respect to d(1/T) at a constant adsorbed quantity (or surface coverage θ).

However, in this study non-linearities were observed in the slope of the isosteres and therefore a quadratic function was parametrized to describe the (1/T) dependency of the ln(p) for each series of data (at a fixed adsorbed quantity). The derivate of each quadratic function was performed at a temperature of T=10 °C to calculate the loading-dependent isosteric heat of adsorption:

$q_i = -d\ln(p)/d(1/T)_\theta R$; q_i = isosteric heat of sorption, R = 8.3144621 J/K/mol

The heat of adsorption for CO_2 is presented as a function of quantity adsorbed in the main manuscript's Figure 11 for both MHH-2 and MHH-4. See Figure S17, Figure S18, Table S4 and Table S5 for further details.

Dubinin-Radushkevich (DR) ultramicropore volume calculations

The used nomenclature is:

V	= adsorbed quantity at equilibrium pressure (cm^3/g STP)
V_o	= micropore capacity (cm^3/g STP)
p_o	= saturation vapor pressure of gas at temperature T (mmHg)
p	= equilibrium pressure (mmHg)
B	= structural constant
β	= convergence coefficient
T	= temperature
MV_{DR}	= Micropore volume (cm^3/g)
D	= density conversion factor = 0.001831 for CO_2 at 0 °C
σ	= molecular cross-sectional area (nm^2) = 0.170 nm^2 for CO_2 at 0 °C

The CO_2 adsorption isotherms recorded at a temperature of 0 °C (adsorbed quantity in cm^3/g (V) plotted as a function of partial pressure (p/p_o)) were used for the DR calculations. p/p_o in the range of 1.24 * 10-5 to 0.02 were used.

The DR equation can be written:

$$\log(V) = \log(V_o) - (B * T)/\beta * (\log(p_o/p))^2$$

Therefore, a plot of log(V) on the Y-axis and $(\log(p_o/p))^2$ on the x-axis can be created, see Figure S12. A linear least squares method was used, where the Y-intercept corresponds to $\log(V_o)$ and the slope corresponds to $-(B * T)/\beta$.

Micropore capacity: $V_o = 10^{\log(Vo)}$

Micropore volume (cm^3/g): $MV_{DR} = V_o * D$

BET surface area calculations

The used nomenclature is:

V	= adsorbed quantity at equilibrium pressure (cm^3/g STP)
p_o	= saturation vapor pressure of gas at temperature T (mmHg)
p	= equilibrium pressure (mmHg)
p/p_o	= relative pressure
S	= slope
$Y_{intercept}$	= Y-intercept
c	= BET constant
V_m	= monolayer adsorbed gas quantity
N	= avogadros number = $6.023*10^{23}$
V_{mol}	= molar volume of adsorbate gas = 22414 cm^3/mol STP
m	= mass of adsorbent (g)
A	= cross-sectional area of adsorbing gas = 0.162 nm^2
S_{BET}	= BET specific surface area (m^2/g)

N_2 adsorption isotherm data collected at -196 °C is used to produce a BET-plot which has $p/(V*(p_o-p))$ on the Y-axis and p/p_o on the X-axis. The points to be used in the BET-plot are here selected as to have $v*(1-p/p_o)$ increasing with increasing p/p_o and a positive c. A linear least squares method is used to yield the Y-intercept and slope in the BET-plot. The BET equation can be written as:

$p/(V(p_o-p)) = (c-1)/(V_m*c) * p/p_o + 1/(V_m*c)$; note: on the form y=kx+m

Therefore, the slope and Y-intercept can be used to solve for c and V_m using the following equations:

$S = (c-1) / (V_m*c)$
$Y_{intercept} = 1 / (V_m*c)$
$V_m = 1/(S+Y_{intercept})$

The BET specific surface area is then calculated according to:
$S_{BET} = (V_m*N*A) / (V_{mol}*m)$

***t*-plot method for calculation of external surface area, micropore volume and micropore surface area**

The used nomenclature is:

t_i	= thickness for the i:th point (Å)
p_i	= pressure for the i:th point (mmHg)
p_o	= saturation vapor pressure of gas at temperature T (mmHg)
p	= equilibrium pressure (mmHg)
p/p_o	= relative pressure
V	= adsorbed quantity at equilibrium pressure (cm^3/g STP)
S	= slope (cm^3/g-Å STP)
$Y_{intercept}$	= Y-intercept
S_{ext}	= external surface area (m^2/g)
S_{mic}	= micropore surface area (m^2/g)
S_{BET}	= BET specific surface area (m^2/g)
V_{mic}	= micropore volume (cm^3/g)
V_{liq}	= volume of adsorbed liquid
V_{ads}	= volume of adsorbed gas

N_2 adsorption isotherm data collected at -196 °C was used. The thickness of the adsorbed layer for each data point can be calculated according to ASTM standard D-6556-10 for carbon black.[27,28]

$$t_i = 0.88*(p_i/p_o)^2 + 6.45*(p_i/p_o) + 2.98$$

A plot with t_i on X-axis and V on the Y-axis gave the *t*-plot. Points were selected according to the ASTM standard for relative pressures 0.2-0.5, corresponding to t-values of 4.3-6.4. A linear least-squares method was used on these points to yield the Y-intercept and the slope. See Figure S20. For N_2 adsorption at -196 °C, the volume of adsorbed liquid is $V_{liq} = 15.47 * V_{ads}$ and therefore:

$$S_{ext} = S * 15.47$$
$$S_{mic} = S_{BET} - S_{ext}$$
$$V_{mic} = Y_{intercept} * 0.001547$$

The equation for the calculation of the thickness of the adsorbed layer is different for different material types. One other commonly used equation is the Harkins-Jura equation (for Al_2O_3), presented below with a comparison of the result to that for the equation for carbon black.

$$t_i = (13.99/(0.034-\log(p_i/p_o))^{1/2}$$

For the same used relative pressure range, there is only a slight difference:

$V_{mic,\ MHH\text{-}4,\ carbon\ black} = 0.350\ cm^3/g$	$V_{mic,\ MHH\text{-}4,\ Harkins\text{-}Jura} = 0.348\ cm^3/g$
$S_{ext,\ MHH\text{-}4,\ carbon\ black} = 173.56\ cm^2/g$	$S_{ext,\ MHH\text{-}4,\ Harkins\text{-}Jura} = 177.05\ cm^2/g$

Note: The selection of the relative pressure range may be ambiguous.

Total pore volume calculation

The used nomenclature is:

V_{tot}	= total pore volume (cm^3/g)
V	= adsorbed quantity at equilibrium pressure (cm^3/g STP)
p_o	= saturation vapor pressure of gas at temperature T (mmHg)
p	= equilibrium pressure (mmHg)
p/p_o	= relative pressure
V_{mol}	= molar volume of adsorbate gas = 22414 cm^3/mol STP
M_{N_2}	= molecular weight of N_2 = 28.01 g/mol
d_{N_2}	= density of liquid N_2 = 0.807 g/cm^3

N_2 adsorption isotherm data collected at -196 °C was used. For the highest relative pressure point recorded ($p/p_o = 0.98$), the adsorbed quantity of N_2 was used to calculate the total pore volume:

$$V_{tot} = V / V_{mol} * M_{N_2} / d_{N_2} = V * 0.001547$$

References

(1) Hara, M.; Yoshida, T.; Takagaki, A.; Takata, T.; Kondo, J. N.; Hayashi, S.; Domen, K. A Carbon Material as a Strong Protonic Acid. *Angew. Chemie - Int. Ed.* **2004**, *43* (22), 2955–2958.

(2) Guo, F.; Xiu, Z. L.; Liang, Z. X. Synthesis of Biodiesel from Acidified Soybean Soapstock Using a Lignin-Derived Carbonaceous Catalyst. *Appl. Energy* **2012**, *98*, 47–52.

(3) Shrestha, R. M.; Varga, I.; Bajtai, J.; Varga, M. Design of Surface Functionalization of Waste Material Originated Charcoals by an Optimized Chemical Carbonization for the Purpose of Heavy Metal Removal from Industrial Waste Waters. *Microchem. J.* **2013**, *108*, 224–232.

(4) Liang, X.; Yang, J. Synthesis of a Novel Carbon Based Strong Acid Catalyst through Hydrothermal Carbonization. *Catal. Letters* **2009**, *132* (3–4), 460–463.

(5) Girisuta, B.; Janssen, L. P. B. M.; Heeres, H. J. A Kinetic Study on the Decomposition of 5-Hydroxymethylfurfural into Levulinic Acid. *Green Chem.* **2006**, *8*, 701.

(6) Van Zandvoort, I.; Wang, Y.; Rasrendra, C. B.; Van Eck, E. R. H.; Bruijnincx, P. C. a; Heeres, H. J.; Weckhuysen, B. M. Formation, Molecular Structure, and Morphology of Humins in Biomass Conversion: Influence of Feedstock and Processing Conditions. *ChemSusChem* **2013**, *6* (9), 1745–1758.

(7) Sumerskii, I. V.; Krutov, S. M.; Zarubin, M. Y. Humin-like Substances Formed under the Conditions of Industrial Hydrolysis of Wood. *Russ. J. Appl. Chem.* **2010**, *83* (2), 320–327.

(8) Hoang, T. M. C.; van Eck, E. R. H.; Bula, W. P.; Gardeniers, J. G. E.; Lefferts, L.; Seshan, K. Humin Based By-Products from Biomass Processing as a Potential Carbonaceous Source for Synthesis Gas Production. *Green Chem.* **2015**, *17* (2), 959–972.

(9) Luijkx, G. C. a; van Rantwijk, F.; van Bekkum, H. Hydrothermal Formation of 1, 2, 4-Benzenetriol from 5-Hydroxymethyl-2-Furaldehyde and D-Fructose. *Carbohydr. Res.* **1993**, *242* (C), 131–139.

(10) Baugh, K. D.; McCarty, P. L. Thermochemical Pretreatment of Lignocellulose to Enhance Methane Fermentation: I. Monosaccharide and Furfurals Hydrothermal Decomposition and Product Formation Rates. *Biotechnol. Bioeng.* **1988**, *31* (1), 50–61.

(11) Rice, J. a.; MacCarthy, P. Statistical Evaluation of the Elemental Composition of Humic Substances. *Org. Geochem.* **1991**, *17* (5), 635–648.

(12) Nam, H.; Wang, S.; Jeong, H. R. TMA and H2S Gas Removals Using Metal Loaded on Rice Husk Activated Carbon for Indoor Air Purification. *Fuel* **2018**, *213* (October 2017), 186–194.

(13) Guo, J.; Xu, W. S.; Chen, Y. L.; Lua, A. C. Adsorption of NH3 onto Activated Carbon Prepared from Palm Shells Impregnated with H2SO4. *J. Colloid Interface Sci.* **2005**, *281* (2), 285–290.

(14) Yagmur, E.; Ozmak, M.; Aktas, Z. A Novel Method for Production of Activated Carbon from Waste Tea by Chemical Activation with Microwave Energy. *Fuel* **2008**, *87* (15–16), 3278–3285.

(15) Aygün, a.; Yenisoy-Karakaş, S.; Duman, I. Production of Granular Activated Carbon from Fruit Stones and Nutshells and Evaluation of Their Physical, Chemical and Adsorption Properties. *Microporous Mesoporous Mater.* **2003**, *66* (2–3), 189–195.

(16) Hao, W.; Björnerbäck, F.; Trushkina, Y.; Oregui Bengoechea, M.; Salazar-Alvarez, G.; Barth, T.; Hedin, N. High-Performance Magnetic Activated Carbon from Solid Waste from Lignin Conversion Processes. 1. Their Use As Adsorbents for CO 2. *ACS Sustain. Chem. Eng.* **2017**, *5* (4), 3087–3095.

(17) Sevilla, M.; Falco, C.; Titirici, M.-M.; Fuertes, A. B. High-Performance CO2 Sorbents from Algae. *RSC Adv.* **2012**, *2* (33), 12792.

(18) Wahby, A.; Ramos-Fernández, J. M.; Martínez-Escandell, M.; Sepúveda-Escribano, A.; Silvestre-Albero, J.; Rodríguez-Reinoso, F. High-Surface-Area Carbon Molecular Sieves for Selective CO2 Adsorption. *ChemSusChem* **2010**, *3* (8), 974–981.

(19) Sevilla, M.; Fuertes, A. B. Sustainable Porous Carbons with a Superior Performance for CO2 Capture. *Energy Environ. Sci.* **2011**, *4* (5), 1765.

(20) Creamer, A. E.; Gao, B. Carbon-Based Adsorbents for Postcombustion CO2 Capture: A Critical Review. *Environ. Sci. Technol.* **2016**, *50* (14), 7276–7289.

(21) Lee, S. Y.; Park, S. J. A Review on Solid Adsorbents for Carbon Dioxide Capture. *J. Ind. Eng. Chem.* **2015**, *23*, 1–

11.

(22) Wang, W.; Zhou, M.; Yuan, D. Carbon Dioxide Capture in Amorphous Porous Organic Polymers. *J. Mater. Chem. A Mater. energy Sustain.* **2017**, *5*, 1334–1347.

(23) Samanta, A.; Zhao, A.; Shimizu, G. K. H.; Sarkar, P.; Gupta, R. Post-Combustion CO2 Capture Using Solid Sorbents: A Review. *Ind. Eng. Chem. Res.* **2012**, *51* (4), 1438–1463.

(24) Deng, S.; Wei, H.; Chen, T.; Wang, B.; Huang, J.; Yu, G. Superior CO2 Adsorption on Pine Nut Shell-Derived Activated Carbons and the Effective Micropores at Different Temperatures. *Chem. Eng. J.* **2014**, *253*, 46–54.

(25) Alabadi, A.; Razzaque, S.; Yang, Y.; Chen, S.; Tan, B. Highly Porous Activated Carbon Materials from Carbonized Biomass with High CO2 Capturing Capacity. *Chem. Eng. J.* **2015**, *281*, 606–612.

(26) Xu, C.; Hedin, N. Microporous Adsorbents for CO2 Capture – a Case for Microporous Polymers? *Mater. Today* **2014**, *17* (8), 397–403.

(27) Lowell, S.; Shields, J. E.; Thomas, M. A.; Thommes, M. *Characterization of Porous Solids and Powders: Surface Area, Pore Size and Density*; 2004; Vol. 16.

(28) ASTM International. *Standard Test Method for Carbon Black — Total and External Surface Area by Nitrogen*; 2012; Vol. D6556.